Intra-atomic frequency-comb-based photonic quantum memory using single-atom-cavity setup

Chanchal ⬡, G. P. Teja, and Sandeep K. Goyal ⬡[*]

Department of Physical Sciences, Indian Institute of Science Education and Research, Mohali, Punjab 140306, India

On-demand and efficient storage of photons is an essential element in quantum information processing and long-distance quantum communication. Most of the quantum memory protocols require bulk systems in order to store photons. However, with the advent of integrated photonic chip platforms for quantum information processing, on-chip quantum memories are highly sought after. In this paper, we propose a protocol for multimode photonic quantum memory using only a single-atom-cavity setup. We show that a single atom containing a frequency comb coupled to an optical cavity can store photons efficiently. Further, this scheme can also be used to store polarization states of light. As examples, we show that rubidium and cesium atoms coupled to nanophotonic waveguide cavities can serve as promising candidates to realize our scheme. This provides the possibility of a robust and efficient on-chip quantum memory to be used in integrated photonic chips.

I. INTRODUCTION

A photonic quantum memory is a device that can store and reemit photons on demand [1–3]. It is an essential component in quantum information processing applications such as quantum networks [4,5], quantum repeaters [6,7], and long-range quantum communication [8]. In a typical atomic-ensemble-based quantum memory, a weak light pulse is absorbed as delocalized atomic excitation over all the atoms in the ensemble. This collective atomic excitation is then transferred to a long-lived spin state of the atoms using control pulses. In order to retrieve the photons from the atomic ensemble, a trigger pulse is used to transfer the excitation from the long-lived spin state to the excited state of the atom, which emits the photons at a desired time [2,3].

Some of the commonly used quantum memory protocols are electromagnetically induced transparency [9–12], controlled reversible inhomogeneous broadening [13–16], gradient echo memory [17–19], Raman memory [20–22], and photon echoes using an atomic frequency comb (AFC) [23–26] and an intra-atomic frequency comb (IAFC) [27–29]. All these techniques use a large ensemble of atoms or bulk materials to store photons.

To gain scalability and the practical advantage in quantum information processing, many efforts are being devoted towards integrated photonic chips [30–37]. On-chip single-photon sources, on-chip beam splitters, and on-chip photon detectors are already available on integrated platforms [38–42], while on-chip quantum memory is still a work in progress and is a highly sought after device [43,44]. Atomic-ensemble-based quantum memories pose challenges for their on-chip integration. So far only the AFC-based quantum memory protocol has been repurposed for on-chip implementation [43,44]. Further, the Raman quantum memory protocol

has been extended to a single-atom level which can potentially be used on integrated photonic chips [45].

In this paper, we propose a scheme for storing weak light pulses and single photons using a single atom coupled to an optical cavity. The trapped atom contains an IAFC. We show that this joint single-atom-cavity setup results in a photon echo, similar to the IAFC-based quantum memory protocol [27]. The efficiency of storing the light in this setup depends on the finesse of the optical cavity and the quality of the frequency comb. We can also achieve robust and efficient storage for polarization and time-bin qubits using this setup. As examples, we show that cesium and rubidium atoms coupled to nanophotonic waveguide cavities can serve as promising candidates for the implementation of this quantum memory protocol.

In principle, the efficiency of this protocol can reach up to 100%, whereas in AFC and IAFC protocols the maximum efficiency in the forward propagation can be only 54%. This is because, unlike in the bulk AFC and IAFC protocols, the reabsorption of the photon in the reemission process is eliminated by keeping the atom-cavity setup in the Purcell regime and using only one atom to store the light.

One of the biggest advantages of the proposed scheme is that it provides a possible realization of an on-chip quantum memory. Furthermore, since our protocol requires only a frequency comb coupled to a cavity, it can also be implemented using the quantum dots inside a cavity [46–49]. On-demand single-photon sources have already been realized using quantum dots [38,40,50,51]. Combining these two can pave the way for efficient on-chip photonic quantum computation.

This paper is organized as follows: In Sec. II we introduce the relevant background required for our results. In Sec. III, we present our result, where we show the photonic quantum memory using a single atom trapped inside an optical cavity. The examples of rubidium and cesium atoms for the implementation of the quantum memory are also presented in this section. We conclude in Sec. IV.

_____
[*]skgoyal@iisermohali.ac.in

II. BACKGROUND

In this section, we introduce the IAFC-based quantum memory protocol and the dynamics of an atom-cavity setup interacting with electromagnetic field.

A. Intra-atomic frequency comb

In IAFC-based quantum memory, we consider an atom with degenerate ground and excited hyperfine levels. This degeneracy is lifted by applying an external magnetic field which results in multiple ground and excited states. All these multiple dipole-allowed transitions considered together result in a comblike structure known as the IAFC [27].

The interaction picture Hamiltonian for an atom that exhibits an IAFC, interacting with electric field $\mathcal{E}(z, t)$ with mean frequency ω_L, reads

$$H = \hbar \sum_{n=1}^{N} \delta_n |e_n\rangle\langle e_n| - \hbar \left[\sum_n \Omega_n(z, t)|e_n\rangle\langle g_n| + \text{H.c.} \right]. \quad (1)$$

We have considered an atom with N ground states $\{|g_n\rangle\}$ and N excited states $\{|e_n\rangle\}$. For simplicity, the transition is allowed only between $|e_n\rangle \leftrightarrow |g_n\rangle$ for all n, and the corresponding transition dipole moment is given by d_n. Here, the Rabi frequency $\Omega_n(z, t) = d_n \mathcal{E}(z, t)/2\hbar$, and $\delta_n = \omega_n^e - \omega_n^g - \omega_L$ is the detuning between the $|e_n\rangle \leftrightarrow |g_n\rangle$ transition frequency and ω_L.

All these dipole-allowed multiple transitions collectively yield a frequency comb. The linewidth of each of the transitions is γ_n, and the mean frequency is $\delta_n + \omega_L$. The spacing between the $(n + 1)$th and nth teeth is given by $\Delta_n = \delta_{n+1} - \delta_n$. For simplicity, we consider an ideal IAFC with uniform comb spacing $\Delta_n \equiv \Delta$ and equal tooth width γ such that the detuning can be written as $\delta_n \equiv n\Delta$.

We consider the absorption of a single photon pulse $\mathcal{E}(0, t)$ with spectral width γ_p in the IAFC such that $\gamma_p \gg \Delta$. If the atom is initially prepared in an equal superposition of multiple ground states, i.e., $|G\rangle = \frac{1}{\sqrt{N}} \sum_n |g_n\rangle$, the initial state for the ensemble of M atoms becomes $|G\rangle^{\otimes M}$. The state of the IAFC at time t after absorbing the single photon pulse can be written as

$$|\psi(t)\rangle \equiv \sum_{j=1}^{M} (\alpha_j |G\rangle^{\otimes(M-1)} |E(t)\rangle_j), \quad (2)$$

where the index j runs over the number of atoms in the ensemble. The state $|E(t)\rangle_j = \frac{1}{\sqrt{N}} \sum_n e^{i\delta_n t} |e_n\rangle_j$ represents collective excited state of the jth atom, and α_j denotes the absorption coefficient of each atom.

The probability of photon emission is given by $P(t) \propto |\langle G| \sum_j S_j |\psi\rangle|^2$, where $S_j = \sum_n |g_n\rangle_j \langle e_n|_j$ is the step-down operator for the jth atom [27]. Using $\delta_n = n\Delta$ in Eq. (2), we see that the probability of photon emission maximizes at $t = 2\pi m/\Delta$ for integer m. The output lights corresponding to different m values are called photon echoes. The time of an echo can be adjusted by changing Δ, which in turn is controlled by the strength of the applied magnetic field. The storage time in IAFC is limited by the peak width γ, which is determined by the natural broadening of the concerned transition.

To achieve on-demand storage using this protocol, the excitation is transferred from the excited level to a spin state with a long lifetime by applying a π pulse before the echo time $2\pi/\Delta$. Applying another π pulse transfers the excitation back to the excited state, causing the photon echo at an appropriate time. The storage time in the case of spin-state transfer is limited by the lifetime of the chosen spin state. Theoretically, a 100% transfer to the spin state is possible if the frequency comb in the excited state is identical to the one in the spin state [27]. However, in the case of realistic systems such as Cs and Rb atoms, it is difficult to find such a perfect spin state. The closest we can get in the case of Cs atoms is the $5p^6 5d$ level [27] with a lifetime of ~ 900 ns. However, since the protocol proposed here works well for quantum dots and other systems as well, one may be able to design a system with near-ideal spin states to yield an on-demand long-time quantum memory.

Another possible method to achieve on-demand storage in IAFCs is based on dynamically changing the magnetic-field interaction. This can be achieved by switching off the magnetic field before the echo time $2\pi/\Delta$ and then switching it on again after an off time T_{off}. Switching off the magnetic field results in freezing of the rephasing process since the energy levels of the ground and excited states become degenerate and the frequency-comb structure disappears, while the rephasing resumes again when the field is switched on again since the frequency comb is restored. This results in an echo time of $2\pi/\Delta + T_{\text{off}}$. The storage time in this method is limited by the lifetime of the excited state of the atomic transition. A similar method based on the approach of freezing and restarting the rephasing dynamics was used in [52].

The efficiency η of the IAFC quantum memory protocol is defined as the ratio of the intensity of light obtained in the first echo to the total intensity of the input light, which reads [27]

$$\eta = \frac{\int_{\pi/\Delta}^{3\pi/\Delta} |\mathcal{E}(z = L, t)|^2 \, dt}{\int |\mathcal{E}(z = 0, t)|^2 \, dt}, \quad (3)$$

where L is the length of the atomic ensemble along the direction of the propagation of light. The maximum efficiency that can be achieved using the standard IAFC scheme is 54% in the forward mode and 100% in the backward mode [27].

B. Dynamics of an atom-cavity system interacting with an electromagnetic field

Consider a two-level atom coupled to an optical cavity. Let $\{|g\rangle, |e\rangle\}$ be the two energy levels of the atom, $\hat{a}$ be the annihilation operator of the cavity mode, and ω_c and ω_{eg} be the cavity-mode frequency and the atomic-transition frequency, respectively. The Hamiltonian for the atom-cavity setup can be written as [53]

$$H = \hbar \omega_c \hat{a}^\dagger \hat{a} + \hbar \omega_{eg} |e\rangle\langle e| - \hbar [g \sigma_{eg} \hat{a} + g^* \sigma_{ge} \hat{a}^\dagger], \quad (4)$$

where $\sigma_{ij} \equiv |i\rangle\langle j|$ represents the transition operators of the two-level atom, $g = \frac{d_{eg}}{\hbar} \sqrt{\frac{\hbar \omega_c}{2\epsilon_0 V}}$ is the coupling constant between the atom and the cavity, and d_{eg} is the transition dipole moment between levels $|e\rangle$ and $|g\rangle$.

The optical cavity is also coupled to an input electromagnetic field mode $\hat{a}_{\text{in}}$ and yields an output mode $\hat{a}_{\text{out}}$ upon interaction of the input field with the cavity. Using the

standard input-output formalism [54], the input, output, and cavity modes are related as

$$\hat{a}_{\text{out}}(t) - \hat{a}_{\text{in}}(t) = \sqrt{\kappa}\,\hat{a}(t), \qquad (5)$$

where κ is the decay rate of the cavity mode at which the photon leaks out from the cavity. Our goal is to calculate the output field mode $\hat{a}_{\text{out}}(t)$ as a function of time for the given input field mode $\hat{a}_{\text{in}}(t)$. In order to achieve that we need to solve for $\hat{a}(t)$. The dynamical equations for the atom-cavity setup can be written as [54]

$$\frac{d}{dt}\hat{a}(t) = \frac{1}{i\hbar}[\hat{a}, H] - \left(\frac{\kappa}{2}\right)\hat{a} - \sqrt{\kappa}\hat{a}_{\text{in}}, \qquad (6)$$

$$\frac{d}{dt}\sigma_{ge}(t) = \frac{1}{i\hbar}[\sigma_{ge}, H] - \left(\frac{\gamma}{2}\right)\sigma_{ge}, \qquad (7)$$

where γ is the free-space spontaneous emission rate of the atom.

The atom-cavity setup is usually operated in two parameter regimes: (i) In the strong-coupling regime the atom-cavity coupling is the highest, i.e., $g \gg \kappa, \gamma$. As a result, the system undergoes a series of damped Rabi oscillations before the photon leaks out of the cavity [53]. (ii) In the bad cavity regime or Purcell regime the cavity decay rate κ is maximum and is characterized by $\kappa > g^2/\kappa > \gamma$ [55]. In the Purcell regime, the atomic decay rate into the cavity mode is enhanced over the free-space decay, as a result of which the atom predominantly decays into the cavity mode with rate $\Gamma_c \sim g^2/\kappa$ on resonance [53]. We use this regime in our protocol since it enables the emission of the photon echo into the cavity mode, and the emitted photon quickly leaks out of the cavity at a rate κ before it can get reabsorbed. In both cases, in order for an efficient atom-photon coupling to occur, the cooperativity parameter $C = g^2/(\kappa\gamma) \gg 1$ [53].

III. RESULTS

The conventional IAFC-based quantum memory scheme uses an ensemble of atoms to store single photons. However, since each atom in IAFC contains a frequency comb, it can be argued that a single atom is capable of storing photons provided the atom and light couple strongly. In principle, one can use a single-mode optical cavity to tune the coupling between the atom and the photons and can realize quantum memory using a single atom. In this section, we explore this feasibility and show that with a proper choice of atom-cavity parameters, one can realize an efficient quantum memory. We also present the implementation scheme using rubidium and cesium atoms coupled to nanophotonic waveguide cavities as examples.

A. Quantum memory using single-atom IAFC coupled to a cavity

Consider an atom that contains a frequency comb coupled to a high-finesse single-mode optical cavity [Fig. 1(a)]. The Hamiltonian for such an atom-cavity system consists of three parts, the free Hamiltonian of the single-mode cavity, the free Hamiltonian of the atom, and the interaction between the two
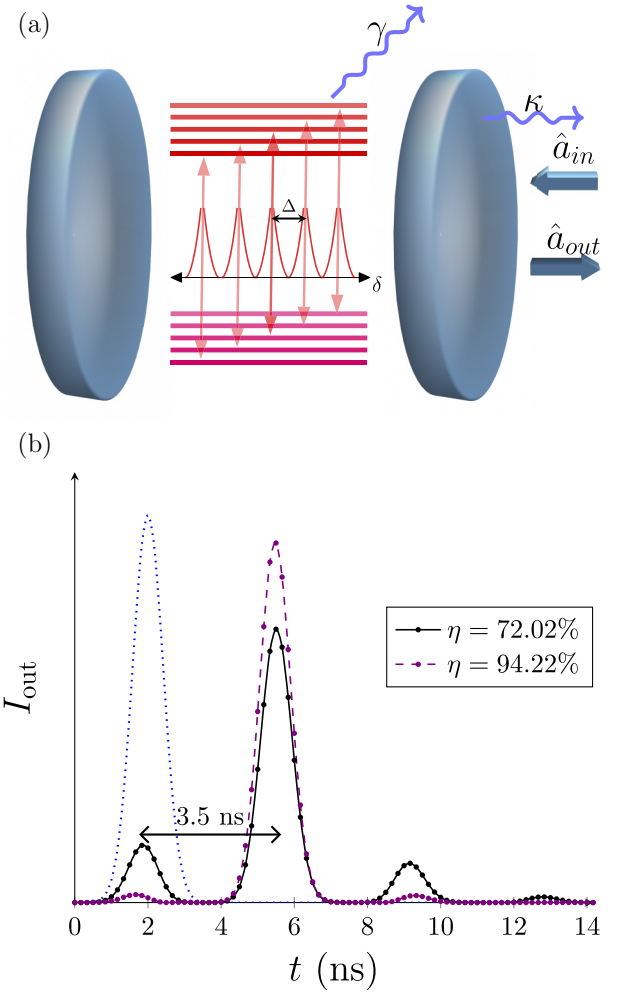

(a)

(b)

FIG. 1. (a) Schematic diagram of an IAFC inside a cavity. Here, the IAFC is interacting with a single cavity mode with decay rate κ. $\hat{a}_{\text{in}}$ and $\hat{a}_{\text{out}}$ represent the input and output field mode operators. γ is the spontaneous decay rate of the atom into free space. (b) Photon echo after a delay of 3.5 ns for an ideal IAFC coupled to a cavity with uniform comb spacing of $\Delta = 2\pi \times 300$ MHz, tooth width $\gamma = 7.5$ MHz, and cavity detuning $\Delta_c = 0$. The input field in Eq. (12) is a Gaussian pulse given by $e^{-\omega^2/(2b^2)}$, with $b = 2\pi \times 270$ MHz. The two photon echoes shown by dashed purple and solid black curves correspond to cavity decay rates of 7 and 4 GHz, respectively, with corresponding efficiencies of 94.22% and 72.02%, respectively. Here, I_{out} represents the rate of photons in the output field (ns^{-1}), which is related to the input field through Eq. (12). The blue dotted curve shows the corresponding input field intensity, $I_{\text{in}} = \langle \hat{a}_{\text{in}}^\dagger(t)\hat{a}_{\text{in}}(t) \rangle$.

systems, which reads

$$\begin{aligned} H &= H_c + H_a + H_{\text{int}} \\ &= \hbar\omega_c \hat{a}^\dagger \hat{a} + \sum_{n=1}^{N} \hbar\omega_n^e |e_n\rangle\langle e_n| + \sum_{n=1}^{N} \hbar\omega_n^g |g_n\rangle\langle g_n| \\ &\quad - \hbar\left[\sum_n g_n |e_n\rangle\langle g_n|\hat{a} + \sum_n g_n^* |g_n\rangle\langle e_n|\hat{a}^\dagger\right], \qquad (8) \end{aligned}$$

where $\hat{a}$ is the photon annihilation operator for the cavity mode. $|g_n\rangle$ and $|e_n\rangle$ denote the nth ground state and the excited state, respectively, with coupling strength $g_n = \frac{d_n}{\hbar}\sqrt{\frac{\hbar\omega_c}{2\epsilon_0 V}}$. d_n is the transition dipole moment of the $|g_n\rangle \leftrightarrow |e_n\rangle$ transition, and ω_c is the resonance frequency of the cavity. Here, it is assumed that a particular ground state $|g_n\rangle$ is coupled only to a single excited state $|e_n\rangle$.

The dynamical equations for the cavity field operator $\hat{a}$ and the atomic lowering operator $\sigma_n^- \equiv |g_n\rangle\langle e_n|$ for a dipole-allowed transition $|g_n\rangle \leftrightarrow |e_n\rangle$ using the input-output formalism as discussed in Sec. II B read

$$\frac{d\hat{a}}{dt} = -i\omega_c\hat{a} + i\sum_{n,m}g_n^*\sigma_n^- - \frac{\kappa}{2}\hat{a} - \sqrt{\kappa}\hat{a}_{\text{in}}, \quad (9)$$

$$\frac{d\sigma_n^-}{dt} = -i(\omega_n^e - \omega_m^g)\sigma_n^- + ig_n(\sigma_{nn}^g - \sigma_{nn}^e)\hat{a} - \frac{\gamma}{2}\sigma_n^-, \quad (10)$$

$$\sqrt{\kappa}\,\hat{a}(t) = \hat{a}_{\text{out}}(t) - \hat{a}_{\text{in}}(t). \quad (11)$$

Here, $\sigma_{nn}^g = |g_n\rangle\langle g_n|$, $\sigma_{nn}^e = |e_n\rangle\langle e_n|$, γ is the spontaneous decay rate of the atom in free space, and κ is the decay rate of the cavity field.

Solving these equations in the frequency domain using the low-intensity approximation ($\langle\hat{a}^\dagger_{\text{in}}\hat{a}_{\text{in}}\rangle \lesssim 1$) which amounts to $\sigma_{nn}^e \approx 0$ [56] yields

$$\hat{a}_{\text{out}}(\omega) = \left[1 - \frac{\kappa}{i(\omega + \Delta_c) + \mathcal{D}(\omega) + \frac{\kappa}{2}}\right]\hat{a}_{\text{in}}(\omega). \quad (12)$$

Here,

$$\mathcal{D}(\omega) = \sum_n \frac{\sigma_{nn}^g|g_n|^2}{\left[i(\omega + \delta_n) + \frac{\gamma}{2}\right]} \quad (13)$$

is the IAFC propagator [27], and $\Delta_c = \omega_c - \omega_L$, $\delta_n = (\omega_n^e - \omega_n^g) - \omega_L$ are the detunings with respect to the input light. The inverse Fourier transform of Eq. (12) yields the output field in time $\hat{a}_{\text{out}}(t)$ [57].

In order for this atom-cavity setup to qualify for a quantum memory, there must be a delay between the input and output light. In Fig. 1(b), we plot the output intensity $I_{\text{out}} = \langle\hat{a}^\dagger_{\text{out}}(t)\hat{a}_{\text{out}}(t)\rangle$ as a function of time, which we get by solving Eq. (12) numerically. Here, we consider a Gaussian input pulse of spectral width $2\pi\times270$ MHz. The IAFC associated with the atom has seven teeth with uniform comb spacing $\Delta = 2\pi\times300$ MHz and tooth width $\gamma = 7.5$ MHz, and the detuning $\Delta_c = 0$. The solid curve and the dashed curve in Fig. 1(b) correspond to two different values of the cavity decay rates κ. In this plot, we can clearly see that the first prominent output pulse of light is at time $t = 2$ ns, which is due to the immediate reflection from the cavity. The second prominent output pulse occurs at $t \sim 5.5$ ns, which is due to the emission from the cavity. There is a delay of 3.5 ns, which is approximately $2\pi/\Delta$ due to the interaction of light with the setup. Hence, the atom-cavity setup behaves like an IAFC.

Equations (12) and (13) suggest that the output field from the atom-cavity setup also depends on the cavity parameters g_n, κ, and Δ_c; hence, they can affect the quality of the memory. To quantify the quality of the quantum memory we can generalize the definition of the efficiency [Eq. (3)] for the bulk
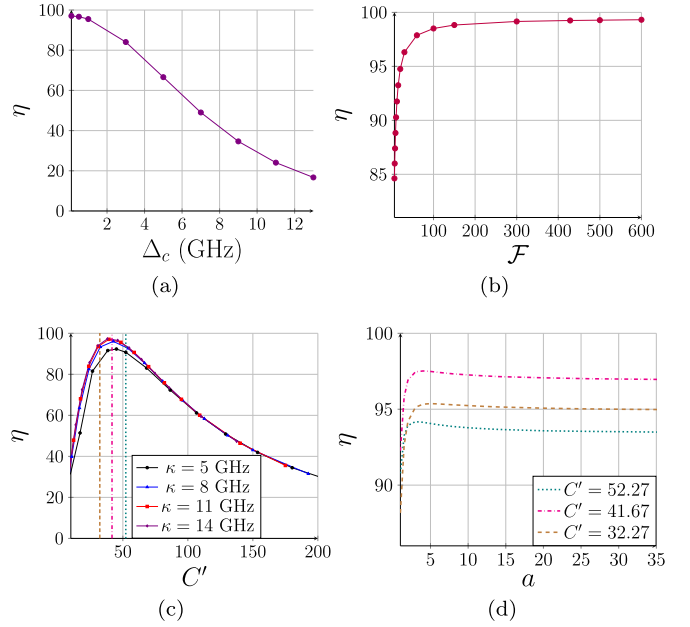

FIG. 2. Effect of various parameters on the efficiency η of quantum memory in the single-atom-cavity setup for an ideal comb. In (a) and (b), we plot the variation of η as a function of the cavity detuning $\Delta_c = \omega_c - \omega_L$ and the comb finesse $\mathcal{F}$, respectively, for $(g', \kappa) = (1.8, 11)$ GHz with uniform comb spacing $\Delta = 2\pi\times300$ MHz. (c) shows the plot of the variation of η as a function of cooperativity, $C' = g'^2/(\kappa\gamma)$, for different values of κ. (d) shows the variation of η as a function of κ given in terms of the parameter a such that $\kappa = a\times5$ GHz for fixed values of cooperativities, as shown by the vertical lines in (c).

IAFC protocol to the current scenario as

$$\eta = \frac{\int_{\pi/\Delta}^{3\pi/\Delta}\langle\hat{a}^\dagger_{\text{out}}(t)\hat{a}_{\text{out}}(t)\rangle\,dt}{\int\langle\hat{a}^\dagger_{\text{in}}(t)\hat{a}_{\text{in}}(t)\rangle dt}. \quad (14)$$

In Fig. 2(a), we plot the variation of the efficiency η as a function of the cavity detuning Δ_c while keeping g' and κ constant. As expected, it shows a drop in the efficiency as the cavity detuning increases. The efficiency also depends on the comb finesse $\mathcal{F} \equiv \Delta/\gamma$. In Fig. 2(b), we plot the efficiency as a function of comb finesse for the ideal comb with fixed comb spacing, $\Delta = 2\pi\times300$ MHz, by changing the peak width γ while keeping the cavity parameters fixed. This plot shows that the efficiency saturates to $\sim100\%$ asymptotically for asymptotic values of the finesse.

Since the storage time is directly controlled by the comb spacing Δ, instead of using the spin-state transfer to increase the storage time, an alternate method would be to decrease the comb spacing Δ, which can be achieved by lowering the applied magnetic field strength. However, reducing Δ reduces the comb finesse ($\mathcal{F} = \Delta/\gamma$), resulting in lower storage efficiencies. In order to preserve the efficiency while decreasing Δ, one can try to preserve $\mathcal{F}$ by reducing the atomic decay rate γ or try to find atomic systems where γ is small.

For an ideal IAFC, since all the peaks are identical, i.e., $d_n \equiv d$, we may write $g_n = g$. We define $g' = g\sqrt{\sigma_{nn}^g}$ as the effective coupling constant and define the cooperativity parameter for the atom-cavity system as $C' = g'^2/(\kappa\gamma)$. In order to understand the effect of the cavity parameters g' and κ on the efficiency, in Fig. 2(c), we plot the variation of η as a function of the cooperativity C' for various values of κ and keeping $\Delta_c = 0$. Figure 2(c) shows that the efficiency first increases, reaches an optimum value, and then starts decreasing, and there exists an optimum value of C' for every given value of κ, which maximizes the efficiency. The maximum efficiencies are obtained in the range $C' \sim 35\text{--}45$ for all the values of κ. Note that in the case of the ensemble-based quantum memories, the efficiency shows a similar behavior with respect to the optical depth and absorption coefficient [27]. Later, we will show the relation between the cooperativity and the absorption using the atom-cavity setup, which will explain the apparent resemblance between the two.

An interesting observation from Fig. 2(c) is that for a fixed value of C' the efficiency increases as we increase κ. In Fig. 2(d), we plot the efficiency as a function of κ while keeping C' fixed. This is achieved by scaling the cavity decay rate κ by a number a and scaling g' by a factor $\sqrt{a}$ so that $C' = g'^2/\kappa\gamma$ remains invariant. Figure 2(d) shows the variation of the efficiency with respect to the parameter a for the three different values of cooperativities corresponding to Fig. 2(c). This shows that for a fixed value of cooperativity C', the efficiency increases with increasing κ and then gets saturated to a constant value. The plot shows a slight dip around $a = 3$ before reaching the saturation. This is because the width of the input pulse is kept fixed while the parameter a varies. Optimizing the efficiency over the input width will result in the saturation of the efficiency without this slight dip. Thus, a combination of the parameters C' and κ determines the optimized efficiency.

So far we have studied numerically the effect of the various parameters on the efficiency of the quantum memory. However, there is a point which remains unexplained. While solving for the output field in Eq. (12), we assumed that there is a negligible absorption of the input field by the atom, i.e., $(\sigma_{nn}^e \sim 0)$, but the efficiency of the storage by this system is still high. To understand this, we consider the expression for the susceptibility χ of the joint atom-cavity system, which reads [58]

$$\chi = \sqrt{\frac{2V}{\epsilon_0 \hbar \omega_c}} \frac{\langle P \rangle}{\langle \hat{a} \rangle}, \tag{15}$$

where $P = \frac{1}{V} \sum_n d_n^* \sigma_n^-$ is the atomic polarization of the atom exhibiting the IAFC and V is the cavity-mode volume. The above expression for susceptibility is equivalent to the classical field susceptibility $\chi_e = \frac{\langle P \rangle}{\epsilon_0 \mathcal{E}}$, where the classical field amplitude $\mathcal{E}$ is replaced by the expectation value of the $\hat{a}$ operator. The susceptibility χ for the IAFC-cavity system can be written as (see Appendix)

$$\chi(\omega) = \frac{2i}{Q} \sum_n \frac{\sigma_{nn}^g |g_n|^2/\kappa}{\left[i(\omega + \delta_n) + \frac{\gamma}{2}\right]}, \tag{16}$$
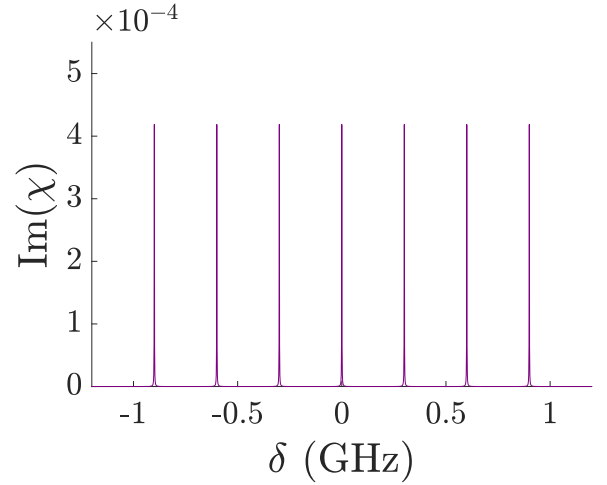

FIG. 3. Plot for absorption of a joint atom-cavity system for an ideal frequency comb with uniform comb spacing $\Delta = 2\pi \times 300$ MHz, tooth width $\gamma = 7.5$ MHz, and cavity detuning $\Delta_c = 0$.

where Q is the quality factor of the cavity given by $Q = \omega_c/\kappa$. The imaginary part of χ gives the absorption for the atom-cavity system.

In Fig. 3, we plot the absorption for the IAFC-cavity system. From Fig. 3, we can see that the absorption profile of the joint atom-cavity system shows a comblike structure similar to the absorption profile in IAFC. This comblike structure is responsible for the photon echo, as shown in Fig. 1(b). Thus, the atom and the cavity together account for the photon storage, even though the absorption by the atom is negligible.

Moreover, as discussed earlier, Eq. (16) clearly shows the direct relation between the absorption and the cooperativity parameter C'. This is similar to the dependence of the absorption in the case of the conventional ensemble-based protocol on the optical depth [27]. Hence, C' can be considered a parameter analogous to the optical depth in the ensemble-based protocol which gives the optimized efficiencies for $C' \sim 35\text{--}45$. This eventually leads to the condition for obtaining the optimized efficiencies given by $\tau C'\gamma \sim 1$, where τ is the input pulse width and γ is the atomic decay rate.

Storing polarization and time-bin qubits. The quantum memory protocol presented here can also be used to store polarization and time-bin photonic qubits. AFC- and IAFC-based quantum memories are known for storing time-bin qubits efficiently [23,59,60]. In time-multiplexing or time-bin qubits a single photon is placed in a superposition of two time bins, say, an early time t and a later time $t + \tau$. Storing these qubits involves storing a single photon arriving at two different times. The corresponding photo echo will occur at $t + 2\pi/\Delta$ and $t + \tau + 2\pi/\Delta$. Since only one photon needs to be stored in this process, our scheme can easily achieve that task. Further, storing polarization states of light in IAFC-based quantum memory was already proposed in [29]. To store polarization qubit, our aim is to store a single photon which is in a superposition of two orthogonal polarizations. This can be achieved using the IAFC-cavity setup

with the single atom consisting of two overlapping frequency combs which satisfy the selection rules corresponding to the two orthogonal polarizations. This results in an independent storage of the two polarization components [29]. Generally, the efficiency and the photon-echo time for the two polarizations can be different. By choosing the cavity parameters appropriately, one can store arbitrary polarization in these systems [29].

To conclude this section, we have shown that a single atom with an IAFC coupled to an optical cavity can store photons efficiently. We have studied the effect of various parameters on the quality of the storage and estimated the optimum values of the parameters for the most efficient storage. The results obtained here are also interesting from a fundamental point of view. We see that even though the IAFC is necessary to store the photons in the atom-cavity system proposed here, the excitation probability of the atom is negligible. The interaction of the IAFC with the cavity yields the comblike absorption profile of the joint atom-cavity system, which enables efficient quantum memory. In the following section, we present examples of systems capable of realizing this quantum memory protocol.

B. Realizing the quantum memory using Rb and Cs atoms

So far, we have discussed the photon storage assuming an ideal frequency comb with uniform comb spacing and the same peak height which interacts with an optical cavity. However, if we consider realistic systems such as Rb and Cs atoms, the frequency combs obtained from them are usually nonuniform with unequal peak heights, which affects the storage process [27,28]. In this section, we discuss the possibilities for experimental implementation of the single-atom-based quantum memory protocol in realistic systems such as Rb and Cs atoms coupled to a nanophotonic waveguide cavity and show that the current scheme can be implemented with the existing experimental techniques.

As discussed in Sec. III A, one of the requirements to achieve efficient quantum memory in the IAFC-cavity setup is a cavity with high coupling strength g of the order of gigahertz (see Fig. 2). This, in turn, requires a cavity with a low mode volume of the order of approximately cubic micrometers. Such strong coupling is difficult to achieve using conventional Fabry-Pérot cavities but can be achieved using nanocavities [61,62] where mode volumes $V \sim \lambda^3$ have already been realized. Apart from this, the strong coupling has been realized in a fiber-based Fabry-Pérot cavity [63] where the mirror surface of the cavity is designed on the optical fiber end faces. This tight confinement using nanophotonic cavities gives an additional advantage of potential integration with nanophotonics. Trapping in such low mode volumes results in atom-cavity strong coupling of the order of g of approximately gigahertz along with the quality factor $Q = \omega_c/\kappa \sim 10^5$ [61].

Although the scheme presented in this paper is applicable to a large class of atoms, molecules, and quantum dots, here, we consider Cs and Rb atoms as examples to realize this quantum memory protocol. The parameters, such as the atomic transitions used in the Cs and Rb atoms, the wavelength,

TABLE I. Rb and Cs parameters used in numerical calculations. λ is the wavelength of transition. B is the magnetic field used in obtaining the IAFC. V, κ, and Q are the mode volume, decay rate, and quality factor of the cavity, respectively.

Atom	Transition	λ (nm)	B (T)	V $(\mu m)^3$	κ (GHz)	Q
Rb [64]	$5s_{1/2} \leftrightarrow 6p_{3/2}$	420.3	0.15	20	~ 7	10^5
Cs [65]	$6s_{1/2} \leftrightarrow 7p_{3/2}$	455.66	0.1	20	~ 8	10^5

the applied magnetic field strength, and so on, for Rb and Cs atoms used for our calculations are given in Table I. In Figs. 4(a) and 4(b), we plot the frequency combs obtained in Rb and Cs atoms. Clearly, these frequency combs are not uniform in comb spacing, nor do they have equal absorption peaks. In Fig. 5(a) we show the photon echo from Rb and Cs atoms calculated numerically by solving Eq. (12). The maximum efficiencies for Rb and Cs atoms are found to be 92.9% and 90.36%, respectively, for the parameters specified in Table I.

Since, in the case of Cs and Rb atoms, each transition $|g_n\rangle \rightarrow |e_n\rangle$ constituting the frequency comb corresponds to a different value of the coupling constant g_n, it is difficult to study the behavior of the efficiency with respect to the cooperativity parameter C'. However, we can consider the variation of the efficiency for Cs and Rb atoms as a function of $1/\kappa$ for fixed g_n and γ, which essentially captures the behavior of the efficiency as a function of the cooperativity. In Fig. 5(b), we plot the variation of the efficiency as a function of $1/\kappa$ for Rb and Cs atoms. It is clear that the trend is similar to that of an ideal comb in Fig. 2(c) with maximum efficiency of $\sim 90\%$. The lower value of the efficiencies in the case of Rb and Cs atoms is due to the inherent nonuniformity present in the frequency combs. This nonuniformity is attributed to different values of the comb spacing Δ_n and the dipole matrix element d_n corresponding to the transition $|e_n\rangle \leftrightarrow |g_n\rangle$. Our calculations show that an efficient quantum memory using a single atom coupled to an optical cavity can be implemented using current experimental techniques.

While solving the dynamics for an IAFC coupled to a cavity, it is assumed that the single atom is at a fixed location. However, there might be an induced light shift when the atom
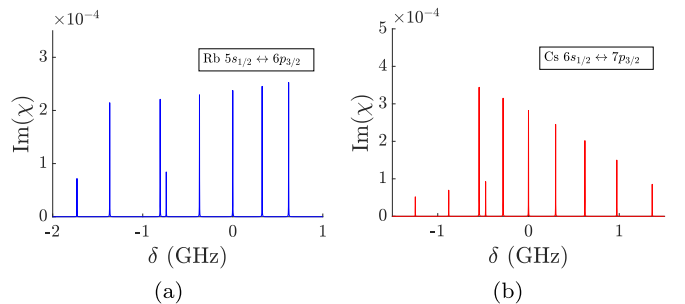

FIG. 4. (a) and (b) represent the frequency comb in Rb and Cs atoms for transitions between $5s_{1/2} \leftrightarrow 6p_{3/2}$ for Rb and $6s_{1/2} \leftrightarrow 7p_{3/2}$ for Cs. The applied magnetic field strengths for Rb and Cs are taken to be 0.15 and 0.1 T, respectively.
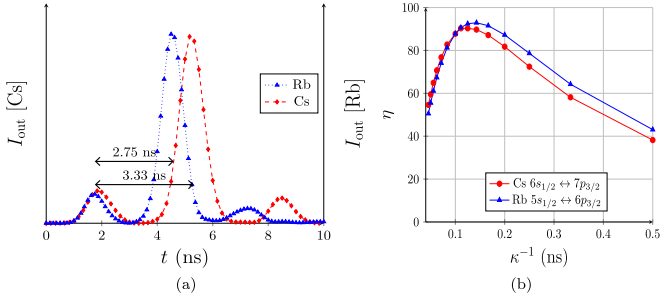
FIG. 5. (a) Photon echo for the IAFC in Rb and Cs atoms. (b) Variation of efficiency as a function of $1/\kappa$ in Rb and Cs atoms.

is trapped using an optical dipole trap. Another factor that can affect the protocol is the spatial inhomogeneous magnetic field. The induced light shift can change the detuning δ_n of the concerned transition $|g_n\rangle \leftrightarrow |e_n\rangle$. Since the detuning of each transition in the frequency comb changes identically, the comb spacing remains the same, and the echo time is not affected. On the other hand, the spatially inhomogeneous field will directly affect the comb spacing of the generated frequency comb. However, there will still be a photon echo at time $2\pi/\Delta'$, where Δ' is the modified comb spacing due to the inhomogeneous magnetic field. To avoid such effects arising from trapping a single atom, one can choose quantum dots or defect centers with a frequency-comb structure.

IV. CONCLUSION

On-chip photonic quantum memories are essential for scalable and integrated photonic quantum information processing. Most of the currently available quantum memory protocols require atomic ensembles or bulk materials to store photons. Here, we have proposed a scheme to store photons using only a single atom coupled to an optical cavity. The atom exhibits an IAFC which enables the joint atom-cavity system to store photons. This provides us with a possibility to realize an on-chip quantum memory suitable for integrated photonic chips. The proposed setup is capable of storing time-multiplexed photons, along with their polarization degree of freedom, efficiently, hence providing multimode photonic quantum memory. Theoretically, our quantum memory protocol can store photons with $\sim$100% efficiency. Although we have presented this quantum memory protocol using trapped atoms, this can work very well with quantum dots and quantum defect centers. The advantage of working with quantum dots and defect centers is that for the case of atoms, the working temperature of the protocol is 10^{-3}–10^{-6} K, whereas this temperature is $\sim$1 K for quantum dots. Since deterministic single-photon sources have already been realized using quantum dots, combining them with the on-chip quantum memory can provide a robust integrated platform for photonic quantum computation.

ACKNOWLEDGMENTS

APPENDIX: SOLVING DYNAMICAL EQUATIONS

To solve Eqs. (9) to (11), we apply the low-intensity approximation ($\langle \hat{a}^\dagger_{\rm in}\hat{a}_{\rm in}\rangle \lesssim 1$), which gives $\sigma^e_{nn} \approx 0$ [56], and introduce the following transformations to go into the rotating frame with respect to the laser frequency ω_L:

$$\hat{a} \rightarrow \tilde{\hat{a}}e^{-i\omega_L t}, \quad \hat{a}_{\rm in} \rightarrow \tilde{\hat{a}}_{\rm in}e^{-i\omega_L t}, \quad \sigma^-_n \rightarrow \tilde{\sigma}^-_n e^{-i\omega_L t}. \quad (A1)$$

Then, Eqs. (9) to (11) can be written as

$$\frac{d\tilde{\hat{a}}}{dt} = -i\Delta_c\tilde{\hat{a}} + i\sum_n g^*_n\tilde{\sigma}^-_n - \frac{\kappa}{2}\tilde{\hat{a}} - \sqrt{\kappa}\tilde{\hat{a}}_{\rm in}, \quad (A2)$$

$$\frac{d\tilde{\sigma}^-_n}{dt} = -i\left(\delta_n - i\frac{\gamma}{2}\right)\tilde{\sigma}^-_n + ig_n\sigma^g_{nn}\tilde{\hat{a}}, \quad (A3)$$

$$\tilde{\hat{a}}_{\rm out}(t) = \sqrt{\kappa}\,\tilde{\hat{a}} + \tilde{\hat{a}}_{\rm in}(t), \quad (A4)$$

where the detunings with the input light are defined as $\Delta_c = \omega_c - \omega_L$ and $\Delta_n = (\omega^e_n - \omega^g_n) - \omega_L$ and $\tilde{\hat{a}}$ and $\tilde{\sigma}^-_n$ are in the rotating frame. Next, we take the Fourier transforms of Eqs. (A2)–(A4) ($t \rightarrow \omega$). The Fourier transform of Eq. (A3) gives

$$\tilde{\sigma}^-_n(\omega) = \frac{ig_n\sigma^g_{nn}}{\left[i(\omega + \delta_n) + \frac{\gamma}{2}\right]}\tilde{\hat{a}}(\omega). \quad (A5)$$

Taking the Fourier transform of Eq. (A2) with respect to t and using Eq. (A5), we get

$$\tilde{\hat{a}}(\omega) = -\frac{\sqrt{\kappa}}{\left[i(\omega + \Delta_c) + \sum_n \frac{\sigma^g_{nn}|g_n|^2}{[i(\omega+\delta_n)+\frac{\gamma}{2}]} + \frac{\kappa}{2}\right]}\tilde{\hat{a}}_{in}(\omega). \quad (A6)$$

Finally, taking the Fourier transform of Eq. (A4) and using Eq. (A6) give the following expression for the output field in the frequency domain:

$$\tilde{\hat{a}}_{\rm out}(\omega) = \left[1 - \frac{\kappa}{i(\omega + \Delta_c) + \mathcal{D}(\omega) + \frac{\kappa}{2}}\right]\tilde{\hat{a}}_{\rm in}(\omega), \quad (A7)$$

where

$$\mathcal{D}(\omega) = \sum_n \frac{\sigma^g_{nn}|g_n|^2}{\left[i(\omega + \delta_n) + \frac{\gamma}{2}\right]}. \quad (A8)$$

Further, the atomic polarization of the single atom exhibiting the IAFC in the frequency domain reads

$$\tilde{P} = \frac{1}{V}\sum_n d^*_n\tilde{\sigma}^-_n, \quad (A9)$$

where V is the cavity-mode volume. Substituting $\tilde{\sigma}_n^-$ from Eq. (A5) and using Eq. (15) gives the following expression for the joint susceptibility χ:

$$\chi(\omega) = \frac{2i}{\omega_c} \sum_n \frac{\sigma_{nn}^g |g_n|^2}{\left[i(\omega + \delta_n) + \frac{\gamma}{2}\right]}. \quad (A10)$$

Further, using the definition of the quality factor, $Q = \omega_c/\kappa$, it can be written as

$$\chi(\omega) = \frac{2i}{Q} \sum_n \frac{\sigma_{nn}^g |g_n|^2/\kappa}{\left[i(\omega + \delta_n) + \frac{\gamma}{2}\right]}. \quad (A11)$$

The imaginary part of χ gives the absorption coefficient for the atom-cavity system.

[1] A. I. Lvovsky, B. C. Sanders, and W. Tittel, Nat. Photon. **3**, 706 (2009).

[2] C. Simon *et al.*, Eur. Phys. J. D **58**, 1 (2010).

[3] K. Heshami, D. G. England, P. C. Humphreys, P. J. Bustard, V. M. Acosta, J. Nunn, and B. J. Sussman, J. Mod. Opt. **63**, 2005 (2016).

[4] H. J. Kimble, Nature (London) **453**, 1023 (2008).

[5] C. Simon, Nat. Photon. **11**, 678 (2017).

[6] Z.-B. Chen, B. Zhao, Y.-A. Chen, J. Schmiedmayer, and J.-W. Pan, Phys. Rev. A **76**, 022329 (2007).

[7] N. Sangouard, C. Simon, H. de Riedmatten, and N. Gisin, Rev. Mod. Phys. **83**, 33 (2011).

[8] L.-M. Duan, M. D. Lukin, J. I. Cirac, and P. Zoller, Nature (London) **414**, 413 (2001).

[9] M. Fleischhauer and M. D. Lukin, Phys. Rev. A **65**, 022314 (2002).

[10] D. Höckel and O. Benson, Phys. Rev. Lett. **105**, 153605 (2010).

[11] Y.-F. Hsiao, P.-J. Tsai, H.-S. Chen, S.-X. Lin, C.-C. Hung, C.-H. Lee, Y.-H. Chen, Y.-F. Chen, I. A. Yu, and Y.-C. Chen, Phys. Rev. Lett. **120**, 183602 (2018).

[12] Y. Wang, J. Li, S. Zhang, K. Su, Y. Zhou, K. Liao, S. Du, H. Yan, and S.-L. Zhu, Nat. Photon. **13**, 346 (2019).

[13] S. A. Moiseev and S. Kröll, Phys. Rev. Lett. **87**, 173601 (2001).

[14] B. Kraus, W. Tittel, N. Gisin, M. Nilsson, S. Kröll, and J. I. Cirac, Phys. Rev. A **73**, 020302(R) (2006).

[15] A. L. Alexander, J. J. Longdell, M. J. Sellars, and N. B. Manson, Phys. Rev. Lett. **96**, 043602 (2006).

[16] N. Sangouard, C. Simon, M. Afzelius, and N. Gisin, Phys. Rev. A **75**, 032327 (2007).

[17] G. Hétet, J. J. Longdell, A. L. Alexander, P. K. Lam, and M. J. Sellars, Phys. Rev. Lett. **100**, 023601 (2008).

[18] M. P. Hedges, J. J. Longdell, Y. Li, and M. J. Sellars, Nature (London) **465**, 1052 (2010).

[19] M. Hosseini, B. M. Sparkes, G. Campbell, P. K. Lam, and B. C. Buchler, Nat. Commun. **2**, 174 (2011).

[20] M. Klein, M. Hohensee, A. Nemiroski, Y. Xiao, D. Phillips, and R. Walsworth, Appl. Phys. Lett. **95**, 091102 (2009).

[21] A. E. Kozhekin, K. Mølmer, and E. Polzik, Phys. Rev. A **62**, 033809 (2000).

[22] J. Guo, X. Feng, P. Yang, Z. Yu, L. Chen, C.-H. Yuan, and W. Zhang, Nat. Commun. **10**, 148 (2019).

[23] M. Afzelius, C. Simon, H. de Riedmatten, and N. Gisin, Phys. Rev. A **79**, 052329 (2009).

[24] M. Afzelius, I. Usmani, A. Amari, B. Lauritzen, A. Walther, C. Simon, N. Sangouard, J. Minář, H. de Riedmatten, N. Gisin, and S. Kröll, Phys. Rev. Lett. **104**, 040503 (2010).

[25] M. Afzelius and C. Simon, Phys. Rev. A **82**, 022310 (2010).

[26] P. Jobez, N. Timoney, C. Laplane, J. Etesse, A. Ferrier, P. Goldner, N. Gisin, and M. Afzelius, Phys. Rev. A **93**, 032327 (2016).

[27] G. P. Teja, C. Simon, and S. K. Goyal, Phys. Rev. A **99**, 052314 (2019).

[28] G. P. Teja and S. K. Goyal, Sci. Rep. **11**, 11439 (2021).

[29] Chanchal, G. P. Teja, C. Simon, and S. K. Goyal, Phys. Rev. A **104**, 043713 (2021).

[30] A. Crespi, R. Ramponi, R. Osellame, L. Sansoni, I. Bongioanni, F. Sciarrino, G. Vallone, and P. Mataloni, Nat. Commun. **2**, 566 (2011).

[31] M. Kohnen, M. Succo, P. Petrov, R. Nyman, M. Trupke, and E. Hinds, Nat. Photon. **5**, 35 (2011).

[32] Y. Meng, J. Lee, M. Dagenais, and S. Rolston, Appl. Phys. Lett. **107**, 091110 (2015).

[33] B. Hacker, S. Welte, G. Rempe, and S. Ritter, Nature (London) **536**, 193 (2016).

[34] S. Freer, S. Simmons, A. Laucht, J. T. Muhonen, J. P. Dehollain, R. Kalra, F. A. Mohiyaddin, F. E. Hudson, K. M. Itoh, J. C. McCallum, D. N. Jamieson, A. S. Dzurak, and A. Morello, Quantum Sci. Technol. **2**, 015009 (2017).

[35] J. G. Titchener, M. Gräfe, R. Heilmann, A. S. Solntsev, A. Szameit, and A. A. Sukhorukov, npj Quantum Inf. **4**, 19 (2018).

[36] A. W. Elshaari, W. Pernice, K. Srinivasan, O. Benson, and V. Zwiller, Nat. Photon. **14**, 285 (2020).

[37] J. Wang, F. Sciarrino, A. Laing, and M. G. Thompson, Nat. Photon. **14**, 273 (2020).

[38] R. Uppu, F. T. Pedersen, Y. Wang, C. T. Olesen, C. Papon, X. Zhou, L. Midolo, S. Scholz, A. D. Wieck, A. Ludwig, and P. Lodahl, Sci. Adv. **6**, eabc8268 (2020).

[39] A. Laucht, S. Pütz, T. Günthner, N. Hauke, R. Saive, S. Frédérick, M. Bichler, M.-C. Amann, A. W. Holleitner, M. Kaniber, and J. J. Finley, Phys. Rev. X **2**, 011014 (2012).

[40] C.-Y. Lu and J.-W. Pan, Nat. Nanotechnol. **16**, 1294 (2021).

[41] S. Yin, H. Qiu, Z. Wang, D. Dai, and X. Guan, Opt. Lett. **47**, 961 (2022).

[42] S. Gyger, J. Zichi, L. Schweickert, A. W. Elshaari, S. Steinhauer, S. F. Covre da Silva, A. Rastelli, V. Zwiller, K. D. Jöns, and C. Errando-Herranz, Nat. Commun. **12**, 1408 (2021).

[43] T. Zhong, J. M. Kindem, J. G. Bartholomew, J. Rochman, I. Craiciu, E. Miyazono, M. Bettinelli, E. Cavalli, V. Verma, S. W. Nam, F. Marsili, M. D. Shaw, A. D. Beyer, and A. Faraon, Science **357**, 1392 (2017).

[44] C. Liu, T.-X. Zhu, M.-X. Su, Y.-Z. Ma, Z.-Q. Zhou, C.-F. Li, and G.-C. Guo, Phys. Rev. Lett. **125**, 260504 (2020).

[45] H. P. Specht, C. Nölleke, A. Reiserer, M. Uphoff, E. Figueroa, S. Ritter, and G. Rempe, Nature (London) **473**, 190 (2011).

[46] A. Kiraz, C. Reese, B. Gayral, L. Zhang, W. Schoenfeld, B. Gerardot, P. Petroff, E. Hu, and A. Imamoglu, J. Opt. B Opt. **5**, 129 (2003).

[47] J. An, A. Franceschetti, and A. Zunger, Nano Lett. **7**, 2129 (2007).

[48] P. Zhang, G. Song, and L. Yu, Photon. Res. **6**, 182 (2018).

[49] D. E. Westmoreland, K. P. McClelland, K. A. Perez, J. C. Schwabacher, Z. Zhang, and E. A. Weiss, J. Chem. Phys. **151**, 210901 (2019).

[50] D. Heinze, D. Breddermann, A. Zrenner, and S. Schumacher, Nat. Commun. **6**, 8473 (2015).

[51] F. Liu, A. J. Brash, J. O'Hara, L. M. P. P. Martins, C. L. Phillips, R. J. Coles, B. Royall, E. Clarke, C. Bentham, N. Prtljaga, I. E. Itskevich, L. R. Wilson, M. S. Skolnick, and A. M. Fox, Nat. Nanotechnol. **13**, 835 (2018).

[52] Z. Bao, Z. Wang, Y. Wu, Y. Li, C. Ma, Y. Song, H. Zhang, and L. Duan, Phys. Rev. Lett. **127**, 010503 (2021).

[53] A. Reiserer and G. Rempe, Rev. Mod. Phys. **87**, 1379 (2015).

[54] C. W. Gardiner and M. J. Collett, Phys. Rev. A **31**, 3761 (1985).

[55] G. S. Agarwal, *Quantum Optics* (Cambridge University Press, Cambridge, 2012)

[56] C. Y. Hu and J. G. Rarity, Phys. Rev. B **91**, 075304 (2015).

[57] G. J. Milburn and S. Basiri-Esfahani, Proc. R. Soc. London A **471**, 20150208 (2015).

[58] Y. Chang, T. Shi, Y.-X. Liu, C. P. Sun, and F. Nori, Phys. Rev. A **83**, 063826 (2011).

[59] M. Gündoğan, P. M. Ledingham, K. Kutluer, M. Mazzera, and H. de Riedmatten, Phys. Rev. Lett. **114**, 230501 (2015).

[60] A. Ortu, A. Holzäpfel, J. Etesse, and M. Afzelius, npj Quantum Inf. **8**, 29 (2022).

[61] D. van Oosten and L. Kuipers, Phys. Rev. A **84**, 011802(R) (2011).

[62] J. D. Thompson, T. Tiecke, N. P. de Leon, J. Feist, A. Akimov, M. Gullans, A. S. Zibrov, V. Vuletić, and M. D. Lukin, Science **340**, 1202 (2013).

[63] D. Hunger, T. Steinmetz, Y. Colombe, C. Deutsch, T. W. Hänsch, and J. Reichel, New J. Phys. **12**, 065038 (2010).

[64] J. E. Sansonetti, J. Phys. Chem. Ref. Data **35**, 301 (2006).

[65] J. Sansonetti, J. Phys. Chem. Ref. Data **38**, 761 (2009).